*19th WORLD CONFERENCE OF THE ASSOCIATED RESEARCH CENTRES FOR THE URBAN UNDERGROUND SPACE*
*Belgrade, Serbia, November 4-7, 2025.*

ACUUS BELGRADE 2025

***Paper No: 2.16.196***
***DOI: 10.46793/ACUUS2025.2.16.196***

# PRELIMINARY NUMERICAL EVALUATION OF RE-USING OIL STORAGE CAVERNS FOR HYDROGEN STORAGE BY USING LINED ROCK CAVERN TECHNOLOGY

**Wenjun Luo[1], Ping Zhang[2], Charlie Chunlin Li[3], Yang Zou[4], Zongze Li[5]**

**Abstract:** The growing demand for large-scale geological hydrogen storage has driven the exploration of innovative and cost-effective methods for repurposing existing underground infrastructure. This study aims to assess the feasibility of converting underground oil storage caverns into Lined Rock Caverns (LRCs) for hydrogen storage. Two construction schemes are proposed and analyzed using numerical simulations, with parameters derived from an existing LRC demonstration project. The maximum allowable gas pressure is determined based on the cavern depth and surrounding rock mass properties, and then the structural response under pressurized conditions is evaluated. The results indicate that the proposed design of dividing original cavern into Multi-caverns using concrete pillars demonstrates favorable structural performance, reducing both the tensile stress level and stress concentration on the steel liner. Meanwhile, the proposed Long-cavern design offers higher hydrogen storage capacity and lower construction costs. In both schemes, the tensile stress level on the steel liner remains low, suggesting significant potential for liner optimization in material selection and liner thickness. These findings confirm the technical feasibility of repurposing oil storage caverns for hydrogen storage and present a sustainable and economically viable solution to meet future energy storage demands.

**Keywords:** Lined rock cavern, Oil storage cavern; Hydrogen storage; Numerical simulation

## 1. INTRODUCTION

Against the backdrop of a global transition toward low-carbon energy systems, hydrogen has emerged as a key component of the future clean energy mix due to its high energy density and zero carbon emissions as a secondary energy carrier (Kovač et al., 2021). With the increasing penetration of renewable energy sources, hydrogen is not only regarded as an effective medium for energy storage but also offers a promising solution to seasonal imbalances in energy supply and demand (Evro et al., 2024). Among the various hydrogen storage methods, underground hydrogen storage has attracted growing attention due to its combined advantages in capacity, cost-effectiveness, and safety (Zhang et al., 2024). In particular, Lined Rock Caverns (LRCs)—a type of underground hydrogen storage structure suitable for hard rock geological formations—create a gas-tight environment through the incorporation of a steel liner and concrete liner, demonstrating strong engineering adaptability and excellent sealing performance (Masoudi et al., 2024).

LRCs rely primarily on the surrounding rock mass to withstand internal gas pressure and prevent structural failure, while the primary function of the liner system is to ensure gas-tight sealing. In the Sweden's project 'Hydrogen Breakthrough Ironmaking Technology', this technology has been tested in Luleå with positive feedback (Vattenfall Press Office, 2025). However, the construction of new LRCs is associated with substantial costs (Papadias and Ahluwalia, 2021). Repurposing unused oil storage caverns for hydrogen storage by using LRCs could eliminate the need for new cavern excavation, thereby significantly reducing costs. To explore the potential role of hydrogen derived from non-fossil sources—as well as hydrogen-based fuels such as ammonia and

1. MSc, Wenjun Luo, Mining and Rock Engineering, PhD Candidate, Department of Civil, Environmental and Natural Resources Engineering, LTU, 97187 Lulea, Sweden, wenjun.luo@ltu.se
2. PhD, Ping Zhang, Mining and Rock Engineering, Professor, Department of Civil, Environmental and Natural Resources Engineering, LTU, 97187 Lulea, Sweden, ping.zhang@ltu.se
3. PhD, Charlie Chunlin Li, Mining and Rock Engineering, Professor, Department of Geoscience and Petroleum, NTNU, Postboks 8900, NO-7491, Trondheim, Norway, charlie.c.li@ntnu.no
4. PhD, Yang Zou, Mining and Rock Engineering, Senior Lecturer, Department of Civil, Environmental and Natural Resources Engineering, LTU, 97187 Lulea, Sweden, yang.zou@ltu.se
5. PhD, Zongze Li, Mining and Rock Engineering, Postdoctoral Fellow, Department of Civil, Environmental and Natural Resources Engineering, LTU, 97187 Lulea, Sweden, zongze.li@associated.ltu.se

methanol—across different types of Nordic ports, the project "*Hydrogen, Ammonia, and Methanol in Hydrogen Hubs in the Nordic Region (H2AMN)*" has been proposed. In this context, it is necessary to investigate the feasibility of converting decommissioned oil storage caverns located near ports into LRCs for storing compressed hydrogen gas. Nevertheless, oil storage caverns typically have a much greater length than width, which poses design challenges for LRC retrofitting. Moreover, the shallow depth of these caverns near ports results in relatively weak confinement from the surrounding rock, making it necessary to calculate the allowable maximum gas pressure and investigate their stability.

Lu (1998) conducted three-dimensional numerical modeling and analyses of LRCs, revealing the roles and stability of the surrounding rock, concrete liner, and steel liner. Johansson (2003) analyzed rock mass deformation and steel liner strain, and proposed a design methodology for storing high-pressure gas in LRCs. Glamheden and Curtis (2006) presented in detail the cavern layout, geometry, and excavation process of the LRC demonstration project in Skallen, Sweden. Based on deformation monitoring data collected during excavation, they conducted a preliminary assessment of post-excavation stability. Damasceno (2022) further investigated the response of the LRC at Skallen to high internal pressure and examined the interactions among different LRC components. Masoudi et al. (2024) discussed the unique challenges of using LRC technology for hydrogen storage and pointed out that the experience in storing high-pressure natural gas in lined rock caverns remains at an early stage. Similarly, in the field of compressed air energy storage, Perazzelli and Anagnostou (2016) performed numerical simulations to analyze uplift failure in shallow caverns. Their results demonstrated that the safety against uplift failure largely depends on rock mass strength, overburden depth, horizontal stress, and cavern type (unlined cavern or shaft), highlighting that the assessment of uplift resistance is a critical aspect of cavern stability evaluation. Therefore, when repurposing shallow-buried caverns into LRCs for high-pressure hydrogen storage, further analysis is required to assess the design parameters and determine the maximum allowable gas pressure, especially considering the typically shallow depth and extended length of such caverns.

Based on the construction experience of LRC demo project at Skallen, Sweden, this study conducts numerical simulations to analyze the behavior of LRCs retrofitted from shallow-buried caverns, using reference parameters such as the surrounding rock properties, cavern geometry, and in-situ stress field from the Skallen project. Two retrofitting schemes are proposed. The first is the Multi-caverns scheme (Scheme I), in which the original unlined cavern is divided into several compartments using concrete pillars, and an LRC is constructed within each compartment. The second is the Long-cavern scheme (Scheme II), in which a single long LRC is constructed along the entire unlined cavern length. To avoid ambiguity, the term "unlined cavern" in this paper refers to an unlined rock cavern with exposed rock surfaces, while "Multi-caverns" and "Long-cavern" specifically denote LRC with concrete or similar liners. Accordingly, the dimensions of the retrofitted cavern are slightly smaller than those of the original unlined cavern. A theoretical model is first developed for the Long-cavern scheme to evaluate the overburden rock's resistance to uplift. Based on unlined cavern dimensions, unlined cavern depth, and rock mass parameters, the maximum allowable gas pressure is calculated. The analysis focuses on rock mass displacement, stress distribution, plastic zones, and tensile stress in the steel liner. Various cavern depths are considered to enhance understanding of their influence on LRC behavior. For the Multi-caverns scheme, the effect of different cavern spacings on cavern performance is examined. The study primarily investigates the mechanical behavior of the two retrofitting schemes under varying cavern depths and compares their respective storage capacities, providing valuable insights for future engineering applications.

## 2. CALCULATION OF MAXIMUM GAS PRESSURE

The internal gas pressure within a LRC can induce uplift of the overburden, making it necessary to evaluate the resistance provided by the overburden against such uplift. In Scheme I, where multiple caverns are located in close proximity, the zones of influence on the overburden induced by gas pressure from each individual caverns partially overlap. Therefore, the worst effect can be approximated by modeling the gas pressure acting on the overburden in a single long cavern, as in Scheme II. The resisting overburden rock mass is illustrated in Figure 1. The resistance against uplift is provided by both the self-weight of the overburden and the tensile strength of the rock mass (Damasceno et al., 2020). For a long cavern, the maximum allowable internal gas pressure can be calculated using the following equation:

$$P_{max} = \frac{\frac{1}{3}\rho \cdot g \cdot d \cdot [A_1 + A_2 + \sqrt{A_1 \cdot A_2}]}{A_2} + \frac{T_0 \cdot (A_1 - A_2)}{A_2} \quad (1)$$

where $P_{max}$ is the maximum gas pressure inside the cavern, $\rho$ is the rock mass density, $g$ is the gravitational acceleration, $d$ is the cavern depth, $A_1$ is the area of the overburden's top surface, $A_2$ is the area of the overburden's bottom surface, and $T_0$ is the tensile strength of the rock mass. $A_1$ can be calculated based on the unlined cavern's length and width, while $A_2$ can be determined from the unlined cavern length, width, depth, and the friction angle $\varphi$ of the rock mass. On the right-hand side of the equation, the first term represents the contribution of the weight

of the overlying rock mass, and the second term accounts for the resistance provided by the tensile strength of the rock.

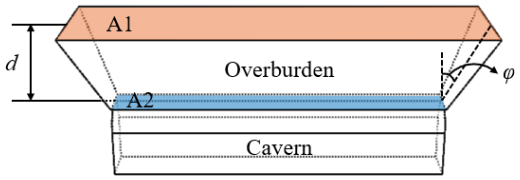


***Figure 1.*** *Overburden of a long cavern.*

## 3. NUMERICAL SIMULATION

This study utilizes FLAC3D for numerical analysis. Based on the shallow-buried, unlined oil storage caverns investigated in the H2AMN project, two schemes are proposed for establishing a three-dimensional numerical model, drawing from existing LRC designs. In the numerical model, different types of elements are used to simulate various LRC components, including the rock mass, concrete liner, steel liner, and sliding layer. Specifically, solid elements are used to model the surrounding rock and concrete liner, while liner structural elements are used to simulate the steel liner. The sliding layer is treated as the interface between the concrete liner and the steel liner. Two schemes are simulated, considering different unlined cavern depths and varying cavern spacings in Scheme I.

### 3.1. Model geometry and boundary conditions

According to the Port of Gothenburg and Port of Piteå, the existing oil caverns are unlined and buried at the depth of 20 to 30 m, and they are usually longer than 100 m, around 20 m in width and about 30 m in height. Based on the basic information provided, a conceptual numerical cavern model with slight small dimension was created with the overburden of 30 m. The unlined cavern is 122 m long, 18 m wide and 25 m high, with the cross-section of a semi-circular arch in the top. After installing the concrete and steel liners, the cross-section of the LRC has a semi-circular geometry in both the top and the bottom. The cross-sections of the cavern and the retrofitted LRC are shown in Figure 2c. Due to the difference in shape between the original unlined and the final lined caverns, the concrete liner thickness becomes uneven along the cavern periphery. Based on the LRC design of the Skallen project in Sweden (Damasceno, 2022), the minimum concrete liner thickness in all models is chosen as 1 m, and the steel liner thickness is set as 0,012 m. For the multiple caverns in Scheme I, the top and bottom of each cavern are semi-spherical with a radius of 8 m, and the middle section is a cylindrical shape with a height of 7 m. The concrete between two adjacent caverns is referred to as the pillar, with the reference thickness of 10 m which is also taken as the cavern spacing in this study and is shown in Figure 2a. For the long cavern in Scheme II, no pillars are placed along the cavern length, as illustrated in Figure 2b, resulting in a LRC length of 120 m.

To investigate the sensitivity of the two schemes to the burial depth, both schemes are compared under two additional unlined cavern depths of 20 m and 40 m. Additionally, in Scheme I, to further assess the impact of cavern spacing, analyses are performed for cavern spacings of 5 m and 2,5 m. All of the simulated cases are summarized in Table 1. M-2 and L-2 are the benchmark cases for Scheme I and Scheme II, respectively, with the corresponding numerical models shown in Figures 2a and 2b.

The in-situ stress in the numerical model is applied based on the stress field evaluated by Glamheden and Curtis (2006), as shown in Table 2. The top of the model represents the ground surface with no constraints. Roller boundary conditions are applied to the sides of the model, and fixed constraints are applied to the bottom. The major horizontal principal stress is parallel to the Y-axis of the numerical model, the minor horizontal principal stress is parallel to the X-axis, and the vertical stress is along the Z-axis of the numerical model.

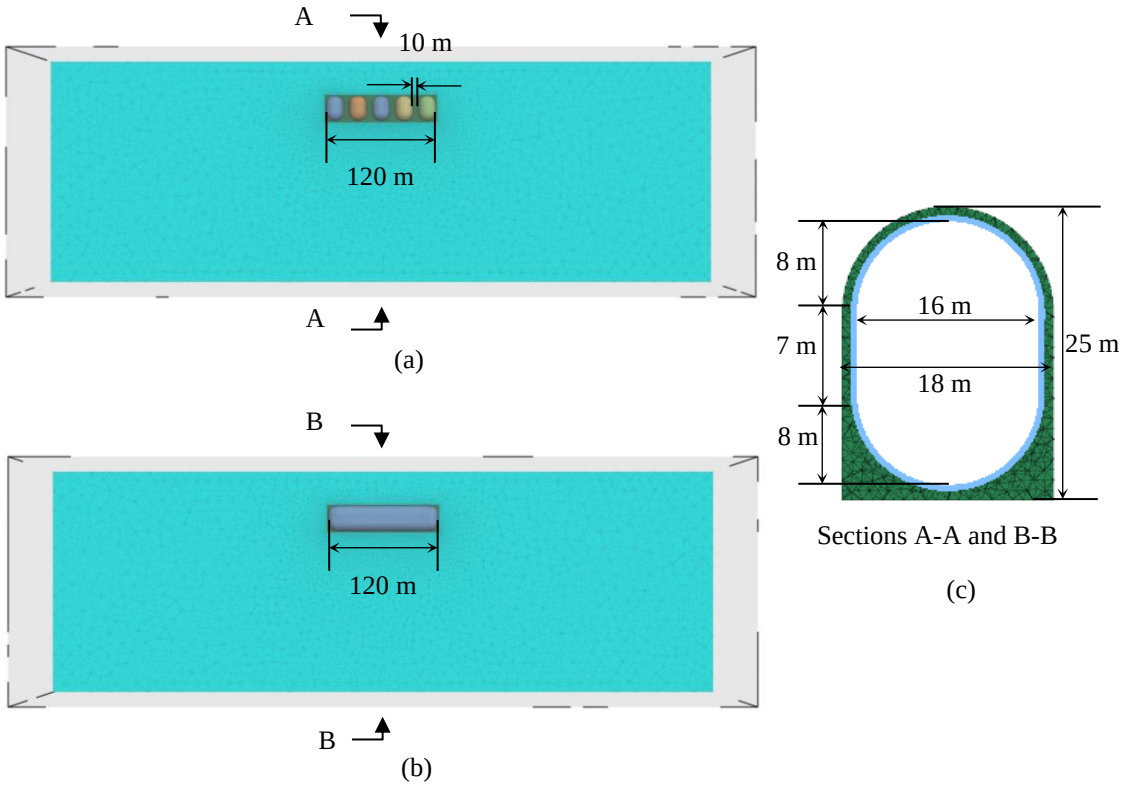


***Figure 2.*** *Numerical models of lined rock caverns for two benchmark cases in two schemes.*

***Table 1.*** *Numerical simulation cases.*

| Case | Scheme | Unlined cavern depth (m) | Cavern spacing (m) | Gas pressure (MPa) |
|---|---|---|---|---|
| M-1 | Multi-caverns | 20 | 10 | P1 |
| M-2 | Multi-caverns | 30 | 10 | P1 |
| M-3 | Multi-caverns | 40 | 10 | P1 |
| L-1 | Long-cavern | 20 | - | P1 |
| L-2 | Long-cavern | 30 | - | P1 |
| L-3 | Long-cavern | 40 | - | P1 |
| M-4 | Multi-caverns | 30 | 5 | P1 |
| M-5 | Multi-caverns | 30 | 2,5 | P1 |

***Table 2.*** *In-situ stress (Glamheden and Curtis 2006).*

| | Value | Unit |
|---|---|---|
| Major horizontal stress ($\sigma_H$) | 0,061$z$-0,32 | MPa |
| Minor horizontal stress ($\sigma_h$) | 0,0295$z$-0,1063 | MPa |
| Vertical stress ($\sigma_V$) | 0,0265$z$ | MPa |

(Note: $z$ means the depth in the numerical model)

***Table 3.*** *Parameters of rock mass, concrete liner and steel liner (Modified after Glamheden and Curtis (2006); Damjanac et al. (2002)).*

| | Parameters | Value | Unit |
|---|---|---|---|
| Rock mass | Density | 2650 | kg/m$^3$ |
| | Elastic modulus | 36 | GPa |
| | Poisson's ratio | 0,25 | |
| | Cohesion | 13,4 | MPa |
| | Tensile strength | 0,4 | MPa |
| | Friction angle | 34 | ° |
| | Dilation angle | 0 | ° |
| Concrete liner | Density | 2400 | kg/m$^3$ |
| | Bulk modulus | 16,7 | GPa |
| | Shear modulus | 12,5 | GPa |
| | Cohesion | 9,6 | MPa |
| | Friction angle | 45 | ° |
| | Tension strength | 2,7 | MPa |
| Steel liner | Elastic modulus | 200 | GPa |
| | Poisson's ratio | 0,3 | |
| | Density | 8000 | kg/m$^3$ |

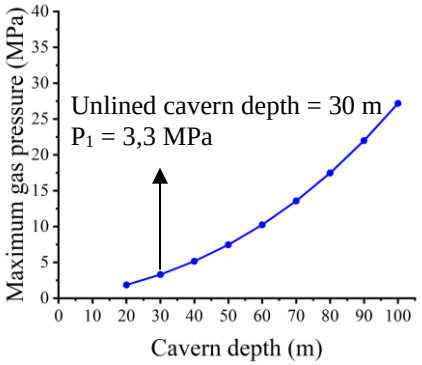


***Figure 3.*** *Relationship between the maximum gas pressure to avoid uplift of overburden and the depth of cavern.*

### 3.2. Constitutive model and parameters

Both the rock mass and concrete use an elasto-plastic constitutive model, while the steel liner is modeled with an elastic constitutive model. The rock mass parameters are set based on the values estimated by Glamheden and Curtis (2006). Since the rock mass may experience tensile failure after the application of gas pressure inside the Lined Rock Cavern, the tensile strength of the rock mass is taken into account. The parameters for concrete and steel liner are referenced from the values provided in the Itasca report (Damjanac et al., 2002). The parameters for the rock mass, concrete, and steel liner are shown in Table 3. Johansson (2003) conducted experimental tests on the bitumen as the sliding layer and monitored the deformation between the steel liner and the concrete in the field. The sliding layer parameters were obtained through calibration, and the shear stiffness is 43 MPa/m and the normal stiffness is 45 GPa/m. The friction coefficient is 0,1.

Based on the input parameters, the maximum gas pressure inside the cavern can be calculated using equation (1). The relationship curve between the cavern depth and maximum gas pressure is shown in Figure 3. As the cavern depth increases, the maximum gas pressure that can be applied inside the lined cavern increases non-linearly. According to the unlined cavern dimensions, depth, rock mass density and friction angle provided above, maximum gas pressure P1 in Table 1 is calculated to be 3,3 MPa.

The numerical model is first subjected to boundary conditions with in-situ stress and displacement constraints. After the in-situ stress is applied, the cavern is excavated and the model is run into equilibrium. Finally, the concrete liner and steel liner are applied, and the corresponding gas pressure is applied to the inner surface of the steel liner and the model reaches the final equilibrium.

## 4. RESULTS AND ANALYSIS

The lined rock cavern primarily relies on a steel liner to contain the compressed, sealed hydrogen gas. Under internal gas pressure, the steel liner experiences tensile stress. If the tensile stress reaches or exceeds the strength of the steel liner, there is a risk of liner failure, which could result in hydrogen leakage. On the other hand, failure of the rock mass and concrete liner can also cause stress concentration on the steel liner, increasing the risk of failure. Additionally, the rock mass failure zone can reflect the risk of uplift in the overburdens of the cavern. This study mainly uses numerical simulations to compare the tensile stress distribution on the steel liner and the failure zones in the rock mass and concrete liner across different cases. Figure 4 shows the sectional distribution of tensile stress on the steel liner in each case, while Figure 5 shows the sectional view of the failure zones in the rock mass and concrete liner. Importantly, the failure zones in the rock mass during the excavation stage and the operation stage (exclude the failure zones from the excavation stage) are summarized and presented in Table 4 for further analysis of the failure zones. In addition, the failure zones within the concrete liner during the operational stage are separately quantified.

### 4.1. Comparison of two benchmark cases

Cases M-2 and L-2 are selected as benchmark cases, with the maximum internal gas pressure determined based on parameters such as rock mass density, friction angle, tensile strength, unlined cavern depth, and unlined cavern geometry. Under internal gas pressure loading, the steel liner is predominantly subjected to tensile stress, while tensile failure primarily occurs in the concrete liner and the surrounding rock mass.

As shown in Figure 4b, the steel liner in Case M-2 exhibits relatively low stress levels, with a maximum tensile stress of 26,2 MPa. Stress concentration occurs near the mid-height and bottom of each cavern, while the stress concentration at the bottom is less pronounced. In contrast, as depicted in Figure 4e, stress concentrations in Case L-2 are observed at both the top and bottom of the steel liner, with more severe concentration at the top. The maximum tensile stress reaches 33,8 MPa at the top and 32,8 MPa at the bottom.

Figure 5b indicates that in Case M-2, the failure zones are relatively limited and are distributed within both the concrete liner and the surrounding rock mass. The damaged zones of concrete liner are primarily located along the flanks of each cavern in the strike direction, with negligible failure zones of rock mass observed at the cavern crown. In contrast, Figure 5e shows that in Case L-2, the failure zones within the concrete liner are more extensive, predominantly concentrated around the crown, invert, and near the cavern ends. The damage zones at the top and bottom of the rock mass in the cave room is relatively large, and it is worth noting that the rock mass near the ground surface also has a lot of damage zones. Further analysis is required by referring to Table 4, which summarizes the volumes of failure zones generated during both the excavation and operational stages. During excavation, both Case M-2 and Case L-2 exhibit some degree of failure in the rock mass. However, in the operational stage, the volume of failure zones in Case M-2 is significantly smaller than that in Case L-2. Similarly, for the concrete liner, the extent of damage during the operational stage in Case M-2 is also much less compared to Case L-2.

On the other hand, from a design perspective, the total volume of the five caverns in Case M-2 is 17.760 $m^3$, with 32.899 $m^3$ of concrete and a steel liner area of 5.781 $m^2$. In contrast, the total volume of the caverns in Case L-2 is 36.110 $m^3$, with 14.549 $m^3$ of concrete and a steel liner area of 7.840 $m^2$. Therefore, Case L-2 requires significantly less investment in these key materials than Case M-2, but in terms of the failure zones, Case M-2 offers greater safety.

### 4.2. Effect of cavern depth

A comparative analysis of Cases M-1, M-2, and M-3 is conducted to evaluate the influence of cavern depth on Scheme I, while Cases L-1, L-2, and L-3 are compared to assess the depth effect on Scheme II.

As shown in Figures 4a, 4b, and 4c, the tensile stress on the steel liner in Scheme I is mainly concentrated in the mid-span and invert regions of the cavern, with peak tensile stresses of 26,6 MPa, 26,2 MPa, and 25,9 MPa, respectively. These results indicate that, in Scheme I, variations in burial depth have a limited effect on the distribution and magnitude of tensile stress in the steel liner.

Figures 5a, 5b, and 5c show that the overall extent of the failure zones increases with burial depth. However, the total volume data at different stages in Table 4 for Cases M-1, M-2, and M-3 reveal that, during the excavation stage, the volume of failure zones in the rock mass increases gradually with burial depth. In contrast, during the operational stage, the volumes of failure zones in both the rock mass and concrete liner are relatively small and tend to decrease with increasing burial depth. Therefore, for Scheme I, under a given internal gas pressure and within a certain burial depth range, greater burial depth has an adverse effect on cavern stability during the excavation but benefits the long-term operation of the LRC.

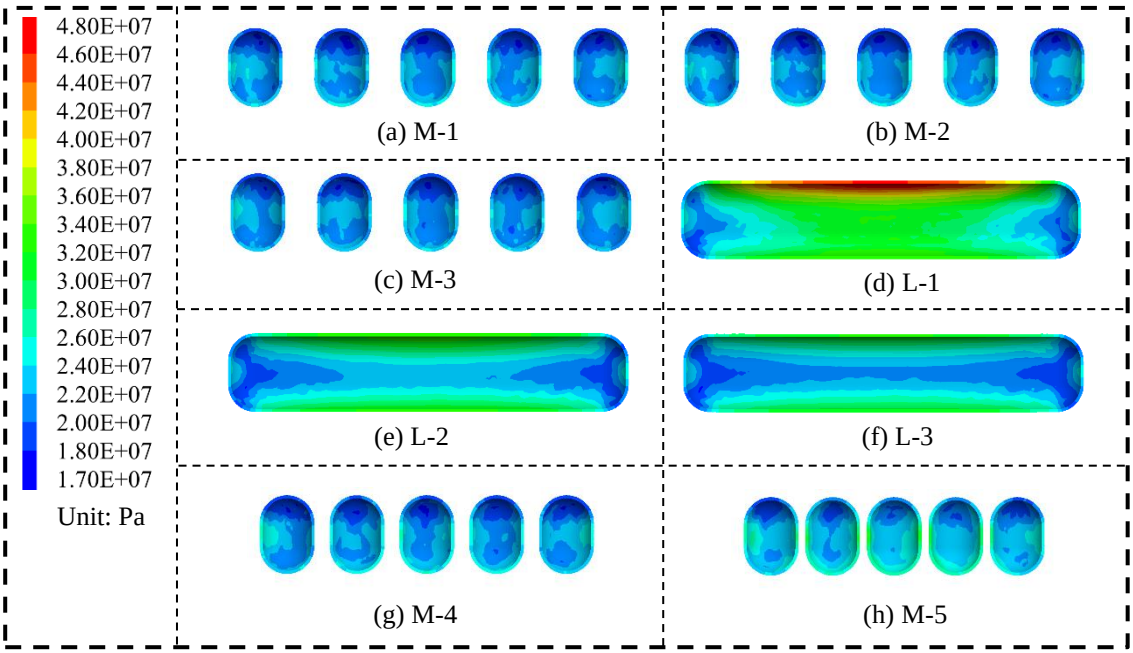


***Figure 4.*** *Tensile stress distribution of steel liner in each case.*

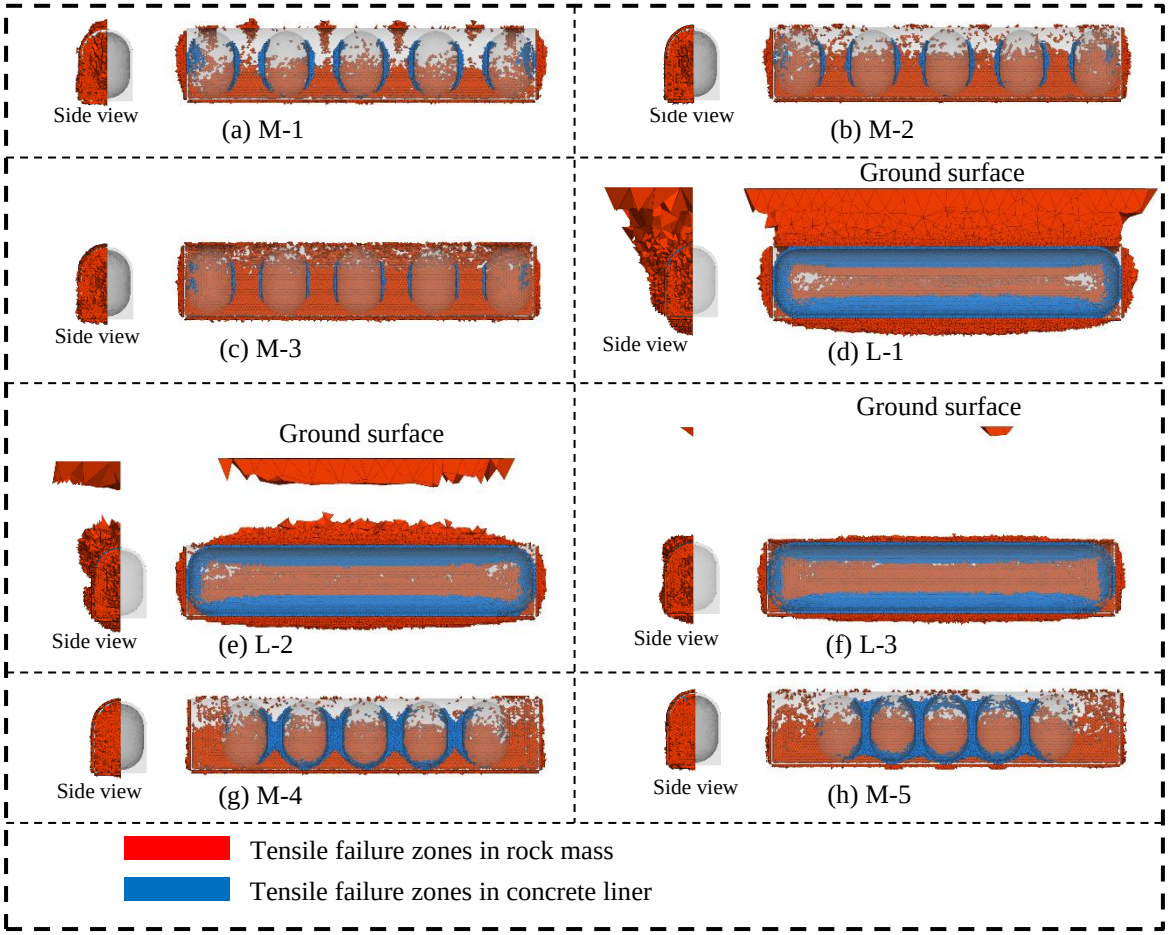


***Figure 5.*** *Failure zones in each case.*

***Table 4.*** *Volume of the failure zones in different stages and materials. (Unit: $m^3$)*

| Stage \ Case / Material | | M-1 | M-2 | M-3 | L-1 | L-2 | L-3 | M-4 | M-5 |
|---|---|---|---|---|---|---|---|---|---|
| Excavation | Rock | 3695,0 | 5427,3 | 6958,2 | 3720,9 | 5398,7 | 7115,7 | 5331,3 | 5411,3 |
| Operation | Rock | 1006,9 | 208,5 | 82,4 | 104572,1 | 35792,9 | 4890,8 | 7,5 | 29,3 |
| | Concrete | 596,0 | 356,7 | 176,0 | 5940,1 | 5449,6 | 5409,6 | 1212,2 | 1777,1 |

In Figures 4d, 4e, and 4f, the tensile stress in the steel liner for Scheme II is mainly concentrated at the cavern crown and the invert, with peak values of 48,0 MPa, 33,8 MPa, and 32,3 MPa, respectively. Stress concentration at the cavern ends is relatively minor. These results suggest that, although burial depth has a limited influence on the stress distribution within the steel liner, the peak tensile stress in Case L-1 is significantly higher than in Cases L-2 and L-3.

As shown in Figures 5d, 5e, and 5f, the extent of the failure zones near the ground surface decreases significantly with increasing depth, and in Case L-1, the failure zones extends from the cavern crown all the way to the ground surface. This indicates that the internal gas pressure in Case L-1 induces significant tensile failure in the overburden, increasing the uplift of the overburden and thereby elevating the risk of LRC failure. According to Table 4, in Scheme II, the failure zones are predominantly generated during the operational stage and tend to decrease with increasing burial depth. In other aspects, the influence of burial depth under a given internal gas pressure in Scheme II is similar to that observed in Scheme I.

In summary, although the maximum tensile stresses in the steel liner are relatively low across all cases, the relatively high tensile stress observed in Case L-1 of Scheme II—along with the extensive tensile failure in both the rock mass and concrete liner I—raises concerns regarding the long-term stability and integrity of the LRC system. Therefore, Scheme I demonstrates better overall stability under shallow burial conditions. On the other hand, the maximum tensile stress in the steel liner decreases with increasing burial depth, and the extent of failure generated during the operational stage also tends to decrease. These observations suggest that increasing the burial depth contributes positively to the stability of the LRC.

### 4.3. Effect of cavern spacing in Scheme I

This section focuses on analyzing the influence of cavern spacing on the performance of the steel liner in Scheme I. A comparison is made among Cases M-2 (benchmark case), M-4, and M-5, all with a burial depth of 30 m. As shown in Figures 4a, 4g, and 4h, the tensile stress in the steel liner increases progressively as the cavern spacing decreases, with peak tensile stresses of 26,2 MPa, 27,9 MPa, and 34,2 MPa, respectively. Figures 5a, 5g, and 5h further reveal that the extent of the failure zones between caverns expands with reduced spacing, and in Cases M-4 and M-5, the failure zones merge between adjacent caverns.

These results indicate that, at a burial depth of 30 m, reducing the cavern spacing leads to increases in both the tensile stress within the steel liner and the extent of the failure zones. Although the increase in tensile stress is relatively modest and remains within a low range in comparison with the steel yielding strength, and no significant tensile failure is observed in the overburden, when a reduced cavern spacing is adopted in Scheme I to lower concrete consumption and construction costs, it is essential to ensure sufficient safety margins.

## 5. DISCUSSION AND CONCLUSIONS

Based on the context of repurposing a shallow and large oil storage cavern for hydrogen storage by using LRC system, this study proposes two preliminary construction options: the Multi-caverns and the Long-cavern schemes. Considering the critical design principle of preventing uplift of the overburden in LRC, an equation was developed to estimate the maximum allowable gas pressure at various cavern depths for a long cavern. The performance of the caverns in the two schemes was then compared under different cavern depths, and the influence of cavern spacing in Scheme I was also investigated. The comparative analysis leads to the following conclusions:

1) The modified rigid cone model estimates maximum gas pressure based on rock mass thickness, internal friction angle, and tensile strength. This model has limitations, as it has not been compared with actual overburden failure. Furthermore, the model's applicability to shallow caverns requires further validation.

2) Scheme I, characterized by smaller cavern volumes and higher concrete consumption, demonstrates better control over failure propagation and liner stress, particularly at shallow depths. In contrast, Scheme II, with larger

cavern volumes and reduced concrete usage, introduces a higher risk of extensive tensile failure in the surrounding rock, especially above the cavern crown. Although the stress levels in the steel liner remain low, the widespread rock mass damage in Scheme II may compromise its long-term performance. Furthermore, the cost factors involved in steel liner welding, concrete construction, support, grouting, and maintenance require further consideration.

3) The influence of burial depth on LRC behavior was evaluated through Cases M-1 to M-3 in Scheme I and Cases L-1 to L-3 in Scheme II. In Scheme I, increased depth had little impact on the tensile stress of steel liner but significantly enlarged failure zones during excavation. However, in the operational stage, both rock mass and concrete liner showed reduced damage with greater depth, indicating that deeper placement benefits long-term performance. In Scheme II, the highest tensile stress and most severe failure occurred in the shallowest case (L-1), suggesting increased risk of gas leakage at low depths. Overall, greater depth improves LRC system stability under both schemes.

4) The effect of cavern spacing was studied in Scheme I through Cases M-2, M-4, and M-5, all at a burial depth of 30 m. Results show that reduced spacing leads to moderately increased tensile stresses in the steel liner and enlarged, even connected, failure zones between caverns. Although the tensile stress remains within safe limits and no significant failure occurs in the overburden, the interaction between adjacent caverns becomes more pronounced. Therefore, when using smaller spacing to reduce material usage and costs, adequate structural reinforcement must be ensured to prevent failure at pillar zones and maintain the integrity of the system.

## 6. ACKNOWLEDGEMENTS

The work has been carried out within the project "Hydrogen, ammonia, and methanol in hydrogen hubs in the Nordic region" with the acronym H2AMN to the Council of Ministers, Nordic Energy Research (NER) (project no. 2315912-0611). The authors gratefully acknowledge the funding from this project and the seed project from CH2ESS, Luleå University of Technology, Sweden.

## 7. REFERENCES

[1] Damasceno D.R. (2022). Modeling aspects of reliability-based design of lined rock caverns. Ph.D. Thesis. Royal Institute of Technology (KTH), Stockholm, Sweden, 85 p.
[2] Damasceno D.R., Spross J. and Johansson F. (2020). Reliability-based design methodology for lined rock cavern depth using the response surface method. ISRM EUROCK. ISRM, 2020.
[3] Damjanac B., Carranza-Torres C. and Dexter R. (2002). Technical review of the LRC concept and design methodology - steel liner response. Itasca Consulting Group, Inc.
[4] Evro S., Oni B.A. and Tomomewo O.S. (2024). Carbon neutrality and hydrogen energy systems. International Journal of Hydrogen Energy. 78, 1449–1467. https://doi.org/10.1016/j.ijhydene.2024.06.407.
[5] Glamheden R. and Curtis P. (2006). Excavation of a cavern for high-pressure storage of natural gas. Tunnelling and Underground Space Technology. 21, 56–67. https://doi.org/10.1016/j.tust.2005.06.002.
[6] Johansson J. (2003). Cavern wall design principles. Licentiate thesis, Royal Institute of Technology (KTH), Stockholm, Sweden, 139 p.
[7] Kovač A., Paranos M. and Marciuš D. (2021). Hydrogen in energy transition: A review. International Journal of Hydrogen Energy. 46, 10016–10035. https://doi.org/10.1016/j.ijhydene.2020.11.256.
[8] Lu M. (1998). Finite element analysis of a pilot gas storage in rock cavern under high pressure. Engineering Geology. 49, 353–361. https://doi.org/10.1016/S0013-7952(97)00067-7.
[9] Masoudi M., Hassanpouryouzband A., Hellevang H. and Haszeldine R.S. (2024). Lined rock caverns: A hydrogen storage solution. Journal of Energy Storage. 84, 110927. https://doi.org/10.1016/j.est.2024.110927.
[10] Perazzelli P. and Anagnostou G. (2016). Design issues for compressed air energy storage in sealed underground cavities. Journal of Rock Mechanics and Geotechnical Engineering, 8(3), 314-328. https://doi.org/10.1016/j.jrmge.2015.09.006.
[11] Papadias D.D. and Ahluwalia R.K. (2021). Bulk storage of hydrogen. International Journal of Hydrogen Energy. 46, 34527–34541. https://doi.org/10.1016/j.ijhydene.2021.08.028.
[12] Vattenfall press office (2025). HYBRIT: Large-scale storage of fossil-free hydrogen gas successfully proven. https://group.vattenfall.com/press-and-media/pressreleases/2025/hybrit-large-scale-storage-of-fossil-free-hydrogen-gas-successfully-proven. 27.02.2025.
[13] Zhang L., Jia C., Bai F., et al. (2024). A comprehensive review of the promising clean energy carrier: Hydrogen production, transportation, storage, and utilization (HPTSU) technologies. Fuel. 355, 129455. https://doi.org/10.1016/j.fuel.2023.129455.